# A theoretical study on the ionic states with analysis of vibrational levels of the photoelectron spectrum of ketene ($C_2H_2O$ and $C_2D_2O$)

Kouichi Takeshita
*Faculty of Bioindustry, Tokyo University of Agriculture, Abashiri, Hokkaido 099-24, Japan*

(Received 20 December 1990; accepted 3 October 1991)

*Ab initio* calculations are performed to study the molecular equilibrium structure and the vibrational levels of the low-lying five ionic states, $1\,^2B_1$, $1\,^2\,^2B_2$, $2\,^2B_1$, $2\,^2B_2$, and $^2A_1$ of ketene ($C_2H_2O$ and $C_2D_2O$.) The theoretical intensity curve obtained by the Franck–Condon factors for the ionization transitions are also reported and compared with the photoelectron spectrum of $C_2H_2O$ and $C_2D_2O$. A number of new assignments of the vibrational levels of the photoelectron spectrum are proposed.

## I. INTRODUCTION

The electronic ground state of ketene is represented by a configuration $\cdots(7a_1)^2(1b_2)^2(1b_1)^2(2b_2)^2(2b_1)^2$ with the $C_{2v}$ symmetry point group.

The photoelectron (PE) spectra of $C_2H_2O$ have been observed in the 9.6–18 eV region where five bands have been found.[1–4] The assignments of the adiabatic ionization energies (AIEs) and the vertical ionization energies (VIEs) have been reported.[1–4] *Ab initio* calculations have given the order of the VIEs as the first $^2B_1$ ($1\,^2B_1$), first $^2B_2$ ($1\,^2B_2$), second $^2B_1$ ($2\,^2B_1$), second $^2B_2$ ($2\,^2B_2$), and $^2A_1$ states.[4–7] The vibrational fine structure have been found in the spectrum of the lower four bands. The assignment of the vibrational fine structure has been discussed.[1–4]

As a molecule is ionized, the equilibrium molecular structure and vibrational mode are changed from those of the ground state. The vibrational structure of the PE spectrum reflects these changes. It is, therefore, interesting to investigate the vibrational structure associated with the change in the equilibrium molecular structure and vibrational mode by ionization. A number of *ab initio* calculations on the equilibrium molecular structure[8–11] and vibrational frequencies[9–11] have been reported. However, many authors have had interest in the ground state. Allen and Schaefer[11] have reported the equilibrium molecular structure and vibrational frequencies of the first ionic state. No *ab initio* investigation of the equilibrium molecular structure and the vibrational fine structure of the higher states has been reported.

In this work, we determined the equilibrium molecular structure of the ground state ($^1A_1$) and five ionic states by using an *ab initio* method. Within the framework of the adiabatic approximation and the harmonic oscillator approximation, we calculated the harmonic force constant matrix elements over variables of totally symmetric distortion and vibrational frequencies of the totally symmetric modes ($\nu_1 \sim \nu_4$). We obtained the approximate theoretical intensity curve using the Franck–Condon factor (FCF). Based on these calculations, we discuss the vibrational fine structure of the ionic states comparing with the PE spectrum of $C_2H_2O$ and $C_2D_2O$.

## II. METHOD OF CALCULATIONS

We used the basis sets of the MIDI-4-type prepared by Tatewaki and Huzinaga.[12] These are augmented by one *p*-type polarization function for *H* and one *d*-type polarization function for C and O. The exponents of the polarization function for *H*, *C* and O are 0.68, 0.61 and 1.16, respectively.

The gradient technique for the Roothaan's restricted Hartree–Fock (RHF) method was employed to determine the optimum molecular structure of the $^1A_1$, $1\,^2B_1$, $1\,^2B_2$, and $^2A_1$ states. The electronic configuration of these states are shown in Table I.

The optimum molecular structure of the $2\,^2B_1$ and $2\,^2B_2$ states were determined by the use of the Newton–Raphson method in which the force and force constant matrix elements were obtained numerically from the total energy. The total energy was calculated by means of a multireference single excitation configuration interaction (MRSCI) method. The reference configurations of the $2\,^2B_1$ and $2\,^2B_2$ states are give in Table I. The reference configurations were

TABLE I. Reference configuration functions.

| State | | Reference function |
|---|---|---|
| $^1A_1$ | ··· | $(6a_1)^2(7a_1)^2(1b_2)^2(1b_1)^2(2b_2)^2(2b_1)^2$ |
| $1\,^2B_1$ | ··· | $(6a_1)^2(7a_1)^2(1b_2)^2(1b_1)^2(2b_2)^2(2b_1)^1$ |
| $1\,^2B_2$ | ··· | $(6a_1)^2(7a_1)^2(1b_2)^1(1b_1)^2(2b_2)^2(2b_1)^2$ |
| $^2A_1$ | ··· | $(6a_1)^1(7a_1)^2(1b_2)^2(1b_1)^2(2b_2)^2(2b_1)^2$ |
| $2\,^2B_1$ | ··· | $(6a_1)^2(7a_1)^2(1b_2)^2(1b_1)^2(2b_2)^2(2b_1)^1$ |
| | | $(6a_1)^2(7a_1)^2(1b_2)^2(1b_1)^1(2b_2)^2(2b_1)^2$ |
| | | $(6a_1)^2(7a_1)^2(1b_2)^2(1b_1)^2(2b_2)^2(3b_1)^1$ |
| | | $(6a_1)^2(7a_1)^2(1b_2)^2(1b_1)^1(2b_2)^2(2b_1)^1(3b_1)^1$ |
| | | $(6a_1)^2(7a_1)^2(1b_2)^2(1b_1)^1(2b_2)^2(3b_1)^2$ |
| | | $(6a_1)^2(7a_1)^2(1b_2)^2(1b_1)^2(2b_2)^1(2b_1)^1(3b_2)^1$ |
| | | $(6a_1)^2(7a_1)^2(1b_2)^2(1b_1)^1(2b_2)^1(2b_1)^2(3b_2)^1$ |
| $2\,^2B_2$ | ··· | $(6a_1)^2(7a_1)^2(1b_2)^1(1b_1)^2(2b_2)^2(2b_1)^2$ |
| | | $(6a_1)^2(7a_1)^2(1b_2)^2(1b_1)^2(2b_2)^1(2b_1)^2$ |
| | | $(6a_1)^2(7a_1)^2(1b_2)^1(1b_1)^2(2b_2)^1(2b_1)^2(3b_2)^1$ |
| | | $(6a_1)^2(7a_1)^2(1b_2)^2(1b_1)^1(2b_2)^1(2b_1)^2(3b_1)^1$ |
| | | $(6a_1)^2(7a_1)^2(1b_2)^2(1b_1)^2(2b_2)^1(2b_1)^1(3b_1)^1$ |
| | | $(6a_1)^2(7a_1)^2(1b_2)^1(1b_1)^2(2b_2)^2(3b_1)^2$ |

 0021-9606/92/021199-11$06.00  

selected so that each weight was greater than 1%. The number of the generated configuration state functions (CSFs) of the $2\ ^2B_1$ and $2\ ^2B_2$ states were 2224 and 2019, respectively.

The single and double excitation configuration interaction (SDCI) method was employed to obtain more accurate ionization energies for the estimation of VIEs and AIEs. For the $^1A_1$, $1\ ^2B_2$, $1\ ^2B_1$, and $^2A_1$ states, a single reference configuration of an SCF wave function of the respective state were employed. For the $2\ ^2B_1$ and $2\ ^2B_2$ states, the multireference configurations were used. In the SDCI method, singly and doubly excited configuration state functions (CSFs) were generated where the inner shells (K shell of C and O) were kept frozen. The generated CSFs were then restricted to the first order interacting space.[13] The number of the generated CSFs of the $^1A_1$, $1\ ^2B_1$, $1\ ^2B_2$, $^2A_1$, $2\ ^2B_1$, and $2\ ^2B_2$ states were 14 543, 14 783, 14 831, 14 921, 97 985, and 89 479, respectively. As the dimensions of the configuration interaction (CI) of the $2\ ^2B_1$ and $2\ ^2B_2$ states were too large, we have adopted a CSF selection process by the use of second-order perturbation theory. The threshold for the selection was $5\mu$hartree. We have estimated the total energy including the contribution from the rejected CSFs by a second-order perturbation theory.[14]

The totally symmetric harmonic force constant matrix elements of the $^1A_1$, $1\ ^2B_2$, $1\ ^2B_1$, and $^2A_1$ states were calculated by means of the gradient technique within the framework of the RHF method. The second derivative was estimated by numerical differentiation of the first derivative. For the $2\ ^2B_1$ and $2\ ^2B_2$ states, we estimated the totally symmetric harmonic force constant matrix elements from a pointwise calculation of the energy obtained by the MRSCI method. We calculated the FCFs only for the totally symmetric modes. The method of calculation of the FCF and theoretical intensity curve was the same as the one used in our previous study.[15]

This work has been carried out by the use of the computer program system GRAMOL[16] for the gradient technique and the calculation of normal modes. (GRAMOL includes the Program JAMOL3 of the RHF calculation part written by Kashiwagi *et al.*[17]) The calculations of the FCF and the theoretical intensity curve have done by the use of the program system FCF&TIC.[18] The program MICA3[19] was used for the CI calculations.

## III. RESULTS AND DISCUSSIONS

The optimized molecular structure of the ground and five cationic states are listed in Table II. The other theoretical results are also presented in Table II. The differences of geometric parameters between the ionic states and the ground state are also given in the parentheses in Table II. An appreciable change occurs in all ionic states. A large geometric change is found in the C = C bond length of the $1\ ^2B_1$ state, in the C = O bond length of the $1\ ^2B_2$, $2\ ^2B_1$, and $2\ ^2B_2$ states and in the H–C = C bond angle of the $2\ ^2B_2$ and $^2A_1$ states.

The optimized molecular structure of the $2\ ^2B_1$ and $2\ ^2B_2$ states were obtained by means of the MRSCI calculations. This is because the RHF calculations were unavailable to the second ionic states. The MRSCI calculations includes correlation effects. Although we cannot calculate the magnitude of correlation effects for the second states, we are able to estimate it for the first ionic states. The correlation energies of the $1\ ^2B_1$ and $1\ ^2B_2$ from the MRSCI calculation are 31% and 19% of the ones from the MRSDCI calculations, respectively.

The total energies at the optimized geometries of the ground and ionic states were calculated by the use of the SDCI method. The weight of each reference function of the $^1A_1$, $1\ ^2B_1$, $1\ ^2B_2$, $2\ ^2B_1$, $2\ ^2B_2$, and $^2A_1$ states at the optimized geometries is 89, 89, 89, 89, 89, and 88%, respectively. The weight of each CSF other than the reference CSF is less than 1%. The VIEs and AIEs of the $1\ ^2B_1$, $1\ ^2B_2$, and $^2A_1$ states were calculated from the energies obtained by means of the single reference SDCI calculations. The VIEs and AIEs of the $2\ ^2B_1$ and $2\ ^2B_2$ states were calculated from differences in energies between the first and second solutions of the MRSDCI calculations. The VIEs and AIEs are listed in Table III. The ordering of the VIEs is the $1\ ^2B_1$, $1\ ^2B_2$, $2\ ^2B_1$, $2\ ^2B_2$, and $^2A_1$ states which is consistent with other results by *ab initio* calculations.[4–7] The ordering of the AIEs is the same as that of VIEs. However, the AIE of $2\ ^2B_2$ is almost

TABLE II. Optimized molecular structure and magnitude of the change in the geometry by ionization. Bond lengths are in angstroms, angles in degrees. The values in parentheses are the magnitude of the change in geometry by ionization. The geometry of the $^1A_1$, $1\ ^2B_1$, $1\ ^2B_2$, and $^2A_1$ states are obtained by RHF method and that of $2\ ^2B_1$ and $2\ ^2B_2$ states are obtained by MRSCI method. Experimental values (Ref.20) of the $^1A_1$ state are as follows: C = O = 1.16 Å, C = C = 1.315 Å, C–D = 1.079 Å, and H–C = C = 118.85°. The other theoretical calculations of the optimized geometry by SCF calculation are follows: For the $^1A_1$ state; (1) C = 0 = 1.1466 Å, C = C = 1.3101 Å, C–H = 1.0735 Å, and H–C = C = 119.01° by Allen and Schaefer (Ref. 11) with double-zeta plus polarization (DPZ) basis set. (2) C = O = 1.168 Å, C = C = 1.305 Å, C–H = 1.072 Å, and H–C = C = 119.3° by Huber and Vogt (Ref. 8) with double-zeta plus floating orbital. For the $1\ ^2B_1$ state; C = 0 = 1.1045 Å, C = C = 1.4120 Å, C–H = 1.075 Å, and H–C = C = 117.63° by Allen and Schaefer (Ref. 11).

| State | C = C (ΔC = C) | C = O (ΔC = O) | C–H (ΔC–H) | H–C = C (ΔH–C = C) |
|---|---|---|---|---|
| $^1A_1$ | 1.310 | 1.140 | 1.079 | 118.99 |
| $1\ ^2B_1$ | 1.406( + 0.096) | 1.095( − 0.045) | 1.085( + 0.006) | 117.69( − 1.30) |
| $1\ ^2B_2$ | 1.257( − 0.052) | 1.296( + 0.155) | 1.096( + 0.017) | 119.58( + 0.59) |
| $2\ ^2B_1$ | 1.351( + 0.041) | 1.276( + 0.135) | 1.081( + 0.003) | 117.37( − 1.62) |
| $2\ ^2B_2$ | 1.318( + 0.008) | 1.234( + 0.094) | 1.128( + 0.049) | 127.91( + 8.92) |
| $^2A_1$ | 1.339( + 0.029) | 1.116( − 0.025) | 1.138( + 0.060) | 96.29( − 22.70) |

TABLE III. Ionization energies (eV). Total energy of $^1A_1$; $-151.564\,055$ a.u. by SCF and $-151.968\,518$ a.u. by SDCI. VIE: Vertical ionization energy. AIE: Adiabatic ionization energy.

| State | VIE | | | AIE | |
|---|---|---|---|---|---|
| | SCF | SDCI | Expt.[a] | SCF | SDCI |
| $1\,^2B_1$ | 8.66 | 9.14 | 9.8 | 8.32 | 8.94 |
| $1\,^2B_2$ | 13.43 | 14.45 | 14.2 | 12.40 | 13.41 |
| $2\,^2B_1$ | ··· | 15.80 | 15.0 | ··· | 14.89 |
| $2\,^2B_2$ | ··· | 16.82 | 16.3 | ··· | 15.92 |
| $^2A_1$ | 16.98 | 16.98 | 16.8 | 15.77 | 15.93 |

[a] Reference 4.

the same value as that of $^2A_1$. The energy lowering of the AIE from the VIE is 0.20, 1.04, 0.91, 0.90, and 1.05 eV for the $1\,^2B_1$, $1\,^2B_2$, $2\,^2B_1$, $2\,^2B_2$, and $^2A_1$ states, respectively.

Table IV contains the calculated vibrational frequencies of the total symmetric modes of the ground and ionic states. The calculated vibrational frequencies of the $^1A_1$ state are compared with the observed values. The calculated values are overestimated by 7%–12%. The present result of the $1\,^2B_2$ state of $C_2H_2O$ is in good agreement with the result from Allen and Schaefer[11] who have calculated by the use of SCF method with double-zeta plus polarization basis sets (see calc.[a] in Table IV).

A conventional potential energy distribution (PED) and a classical half amplitude of the zero-point vibration were calculated in order to characterize each normal mode of $C_2H_2O$. The results are shown in Tables V and VI. Table V shows that each PED of the $\nu_1$ mode has large value in C–H stretching. Thus, all $\nu_1$ modes may be characterized as the C–H stretching mode. From Table V, we should assign the $\nu_2$ mode of $1\,^2B_1$ to the C = O stretching mode, the $\nu_3$ modes of $1\,^2B_1$, $1\,^2B_2$, and $2\,^2B_1$ to the H–C = C bending mode, and the $\nu_4$ mode of $1\,^2B_1$ to the C = C stretching mode. However, the other modes show a coupling among the C = O, C = C, and C–H stretching motions and the H–

TABLE IV. Vibrational frequencies ($cm^{-1}$).

| | State | $\nu_1$ | $\nu_2$ | $\nu_3$ | $\nu_4$ |
|---|---|---|---|---|---|
| $CH_2O_2$ | $^1A_1$ | 3349 | 2372 | 1523 | 1253 |
| | Calc.[a] | 3355 | 2360 | 1537 | 1245 |
| | Obs.[b] | 3070 | 2152 | 1388 | 1118 |
| | $1\,^2B_1$ | 3288 | 2596 | 1471 | 1049 |
| | Calc.[a] | 3305 | 2597 | 1496 | 1024 |
| | $1\,^2B_2$ | 3182 | 2135 | 1337 | 1057 |
| | $2\,^2B_1$ | 3343 | 2125 | 1474 | 1033 |
| | $2\,^2B_2$ | 3215 | 2692 | 1503 | 1127 |
| | $^2A_1$ | 2737 | 2439 | 1335 | 992 |
| $CD_2O_2$ | $^1A_1$ | 2466 | 2335 | 1358 | 993 |
| | Obs.[b] | 2267 | 2120 | 1228 | 927 |
| | $1\,^2B_1$ | 2596 | 2374 | 1153 | 950 |
| | $1\,^2B_2$ | 2368 | 2065 | 1131 | 889 |
| | $2\,^2B_1$ | 2428 | 2111 | 1170 | 925 |
| | $2\,^2B_2$ | 2780 | 2275 | 1263 | 940 |
| | $^2A_1$ | 2454 | 1924 | 1303 | 735 |

[a] Taken from SCF calculations with double-zeta plus polarization (DZP) by Allen and Schaefer (Ref. 11).
[b] Reference 21.

TABLE V. Conventional potential energy distribution (%) of $CH_2O_2$.

| State | | $\nu_1$ | $\nu_2$ | $\nu_3$ | $\nu_4$ |
|---|---|---|---|---|---|
| $^1A_1$ | C = C | 0.9 | 27.9 | 19.0 | 58.1 |
| | C = O | 0.0 | 71.9 | 4.6 | 20.1 |
| | C–H | 99.0 | 0.1 | 0.1 | 0.3 |
| | H–C = C | 0.1 | 0.1 | 76.3 | 21.5 |
| $1\,^2B_1$ | C = C | 0.3 | 9.8 | 4.8 | 93.0 |
| | C = O | 0.0 | 90.2 | 0.0 | 6.8 |
| | C–H | 99.6 | 0.0 | 0.0 | 0.1 |
| | H–C = C | 0.1 | 0.0 | 95.2 | 0.1 |
| $1\,^2B_2$ | C = C | 1.3 | 70.6 | 2.9 | 26.8 |
| | C = O | 0.0 | 27.6 | 8.3 | 65.8 |
| | C–H | 98.6 | 0.6 | 0.0 | 0.1 |
| | H–C = C | 0.1 | 1.2 | 88.8 | 7.3 |
| $2\,^2B_1$ | C = C | 0.5 | 45.4 | 6.0 | 51.4 |
| | C = O | 0.0 | 54.4 | 1.2 | 46.2 |
| | C–H | 99.3 | 0.0 | 0.4 | 0.2 |
| | H–C = C | 0.2 | 0.2 | 92.4 | 2.2 |
| $2\,^2B_2$ | C = C | 0.9 | 30.0 | 28.0 | 31.5 |
| | C = O | 9.8 | 42.3 | 0.1 | 51.1 |
| | C–H | 88.2 | 27.3 | 1.4 | 0.7 |
| | H–C = C | 1.1 | 0.4 | 70.4 | 16.7 |
| $^2A_1$ | C = C | 0.6 | 17.6 | 59.4 | 22.1 |
| | C = O | 2.6 | 77.8 | 10.6 | 2.6 |
| | C–H | 96.8 | 4.6 | 1.2 | 0.2 |
| | H–C = C | 0.0 | 0.1 | 28.9 | 75.1 |

TABLE VI. Classical half amplitude of the zero-point vibrational states of $CH_2O_2$. Bond lengths are in angstroms, angles in degrees.

| State | | $\nu_1$ | $\nu_2$ | $\nu_3$ | $\nu_4$ |
|---|---|---|---|---|---|
| $^1A_1$ | C = C | −0.007 | −0.036 | −0.024 | 0.034 |
| | C = O | 0.001 | 0.044 | −0.009 | 0.015 |
| | C–H | 0.072 | −0.002 | −0.002 | 0.002 |
| | H–C = C | 0.304 | 0.272 | 5.479 | 2.364 |
| $1\,^2B_1$ | C = C | −0.006 | −0.029 | −0.015 | 0.054 |
| | C = O | −0.001 | 0.043 | 0.000 | 0.007 |
| | C–H | 0.073 | 0.001 | −0.001 | 0.001 |
| | H–C = C | 0.288 | −0.020 | 5.975 | 0.156 |
| $1\,^2B_2$ | C = C | −0.008 | 0.048 | −0.008 | 0.020 |
| | C = O | 0.001 | −0.037 | −0.016 | 0.039 |
| | C–H | 0.074 | 0.005 | −0.001 | 0.001 |
| | H–C = C | 0.319 | −0.867 | 5.959 | 1.453 |
| $2\,^2B_1$ | C = C | −0.006 | 0.043 | −0.014 | 0.034 |
| | C = O | −0.000 | −0.043 | −0.006 | 0.030 |
| | C–H | 0.072 | 0.000 | −0.003 | 0.002 |
| | H–C = C | 0.361 | −0.306 | 5.936 | 0.757 |
| $2\,^2B_2$ | C = C | 0.006 | −0.035 | −0.030 | 0.027 |
| | C = O | −0.016 | 0.034 | 0.002 | 0.028 |
| | C–H | 0.066 | 0.037 | −0.007 | 0.004 |
| | H–C = C | 0.749 | −0.434 | 5.176 | 2.127 |
| $^2A_1$ | C = C | 0.006 | −0.033 | −0.043 | 0.022 |
| | C = O | −0.008 | 0.043 | −0.011 | 0.005 |
| | C–H | 0.077 | 0.017 | 0.006 | 0.002 |
| | H–C = C | −0.187 | 0.304 | 3.975 | 5.315 |

C = C bending motion. The $\nu_2$ modes of the $^1A_1$, $1\,^2B_2$, $2\,^2B_1$, and $^2A_1$ states and the $\nu_4$ modes of the $1\,^2B_2$ and $2\,^2B_1$ states show a mixture of the C = O and C = C stretching motions. Table VI shows that the phase of the linear combination of the C = O stretching and the C = C stretching is out of phase for the the $\nu_2$ mode and in phase for the $\nu_4$ mode. Thus, the $\nu_2$ and $\nu_4$ modes of these states may be characterized as the C = C = O out-of-phase stretching and C = C = O in-phase stretching modes, respectively.

Tables VII and VIII show the PED and the classical half amplitude of the zero-point vibration of $C_2D_2O$, respectively. The $\nu_1$ modes of the $^1A_1$, $1\,^2B_2$, and $2\,^2B_1$ states may be characterized as the C–H stretching mode. The $\nu_1$ and $\nu_2$ modes of the $1\,^2B_1$, $2\,^2B_2$, and $^2A_1$ states may be characterized as the C = O and C–H stretching modes, respectively. We should also assign the $\nu_3$ mode of $^2A_1$ to the C = C stretching mode, the $\nu_4$ modes of $^1A_1$, $1\,^2B_2$, and $^2A_1$ to the H–C = C bending mode. However, the other modes show a coupling among the C = O, C = C, and C–H stretching motions and the H–C = C bending motion.

Using the AIEs by the SDCI calculation and the zero-point vibrational energies, we estimated the zero–zero (O–O) IEs. The result is presented in Table IX comparing with the observed values. The calculated O–O IEs of the $1\,^2B_1$, $1\,^2B_2$, $2\,^2B_2$, and $^2A_1$ states of $C_2H_2O$ are underestimated by 0.71, 0.48, 0.16, and 0.83 eV, respectively. The calculated O–O IE of the $2\,^2B_1$ state is overestimated by 0.24 eV. The FCFs of O–O transition are also presented in Table IX. The calculated FCFs of the $1\,^2B_1$, $1\,^2B_2$, $2\,^2B_1$, and $2\,^2B_2$ states are large enough to observe the O–O transition.

Figure 1 shows the overall feature of the theoretical intensity curve (TIC) of $C_2H_2O$ with a half width of 0.08 eV and the observed PE spectrum (PES) from Turner *et al.*[3] A total intensity curve was obtained by using the assumption that the transition probability of the electronic part is the same for each ionic state. The vibrational structure of the TIC is in good agreement with that of the observed PES except for the $1\,^2B_2$ state. The TIC of the $1\,^2B_2$ state appears more resolved than the vibrational structure comparing with the PES of 13.84–14.62 eV. Although the O–O IE of $2\,^2B_1$ is overestimated, the fine structure of TIC mimics the observed

TABLE VII. Conventional potential energy distribution (%) of $CD_2O_2$.

| State | | $\nu_1$ | $\nu_2$ | $\nu_3$ | $\nu_4$ |
|---|---|---|---|---|---|
| | C = C | 16.9 | 13.9 | 57.7 | 11.4 |
| $^1A_1$ | C = O | 16.7 | 59.4 | 16.5 | 4.7 |
| | C–H | 65.8 | 26.7 | 2.6 | 0.1 |
| | H–C = C | 0.7 | 0.0 | 23.2 | 83.8 |
| | C = C | 9.9 | 1.3 | 39.6 | 54.3 |
| $1\,^2B_1$ | C = O | 90.1 | 0.1 | 1.6 | 5.3 |
| | C–H | 0.1 | 98.1 | 0.7 | 0.2 |
| | H–C = C | 0.0 | 0.5 | 58.1 | 40.1 |
| | C = C | 22.7 | 49.3 | 21.2 | 7.3 |
| $1\,^2B_2$ | C = O | 3.8 | 26.1 | 50.6 | 16.9 |
| | C–H | 72.6 | 24.1 | 0.8 | 0.0 |
| | H–C = C | 0.9 | 0.4 | 27.4 | 75.8 |
| | C = C | 5.2 | 41.2 | 27.8 | 28.7 |
| $2\,^2B_1$ | C = O | 0.6 | 55.4 | 17.4 | 29.8 |
| | C–H | 93.5 | 3.2 | 1.8 | 0.1 |
| | H–C = C | 0.7 | 0.3 | 53.0 | 41.3 |
| | C = C | 28.3 | 15.4 | 49.4 | 6.3 |
| $2\,^2B_2$ | C = O | 67.2 | 2.2 | 12.2 | 35.5 |
| | C–H | 4.2 | 81.0 | 7.3 | 0.1 |
| | H–C = C | 0.3 | 1.3 | 31.1 | 58.1 |
| | C = C | 18.4 | 0.2 | 73.1 | 8.8 |
| $^2A_1$ | C = O | 81.2 | 1.2 | 12.4 | 0.8 |
| | C–H | 0.4 | 98.6 | 1.1 | 0.4 |
| | H–C = C | 0.1 | 0.0 | 13.3 | 89.9 |

TABLE VIII. Classical half amplitude of the zero-point vibrational states of $CD_2O_2$. Bond lengths are in angstroms, angles in degrees.

| State | | $\nu_1$ | $\nu_2$ | $\nu_3$ | $\nu_4$ |
|---|---|---|---|---|---|
| | C = C | −0.028 | 0.025 | −0.038 | 0.014 |
| $^1A_1$ | C = O | 0.021 | −0.038 | −0.015 | 0.007 |
| | C–H | 0.052 | 0.032 | −0.007 | 0.001 |
| | H–C = C | 0.652 | 0.041 | 2.789 | 4.266 |
| | C = C | −0.029 | −0.010 | −0.041 | 0.036 |
| $1\,^2B_1$ | C = O | 0.043 | −0.001 | −0.004 | 0.006 |
| | C–H | 0.002 | 0.061 | −0.004 | 0.002 |
| | H–C = C | 0.071 | 0.527 | 4.352 | 2.717 |
| | C = C | −0.029 | 0.039 | −0.020 | 0.010 |
| $1\,^2B_2$ | C = O | 0.015 | −0.035 | −0.038 | 0.018 |
| | C–H | 0.056 | 0.029 | −0.004 | 0.001 |
| | H–C = C | 0.797 | −0.502 | 3.084 | 4.232 |
| | C = C | −0.016 | −0.041 | −0.028 | 0.023 |
| $2\,^2B_1$ | C = O | 0.005 | 0.043 | −0.020 | 0.021 |
| | C–H | 0.060 | −0.010 | −0.006 | 0.001 |
| | H–C = C | 0.653 | 0.362 | 4.171 | 2.953 |
| | C = C | −0.030 | −0.025 | −0.035 | 0.011 |
| $2\,^2B_2$ | C = O | 0.038 | 0.008 | −0.014 | 0.022 |
| | C–H | −0.013 | 0.062 | −0.015 | 0.001 |
| | H–C = C | −0.320 | 0.782 | 3.035 | 3.690 |
| | C = C | −0.033 | −0.003 | −0.047 | 0.012 |
| $^2A_1$ | C = O | 0.044 | 0.005 | −0.012 | 0.002 |
| | C–H | −0.005 | 0.066 | 0.006 | 0.003 |
| | H–C = C | 0.314 | −0.086 | 2.640 | 5.071 |

TABLE IX. O–O ionization states. O–O IE: zero–zero ionization energy. FCF: Franck–Condon factor.

| | | O–O IE(eV) | | | FCF |
|---|---|---|---|---|---|
| | State | This work | Obs.[a] | Obs.[b] | |
| $CH_2O_2$ | $1\,^2B_1$ | 8.93 | 9.64 | 9.63 | 0.231 |
| | $1\,^2B_2$ | 13.36 | 13.84 | 13.84 | 0.011 |
| | $2\,^2B_1$ | 14.86 | 14.62 | 14.60 | 0.007 |
| | $2\,^2B_2$ | 15.92 | 16.08 | 16.08 | 0.024 |
| | $^2A_1$ | 15.87 | ··· | 16.7 | 0.000 |
| $CD_2O_2$ | $1\,^2B_1$ | 8.94 | | 9.63 | 0.226 |
| | $1\,^2B_2$ | 13.37 | | 13.84 | 0.011 |
| | $2\,^2B_1$ | 14.86 | | 14.60 | 0.007 |
| | $2\,^2B_2$ | 15.93 | | 16.08 | 0.012 |
| | $^2A_1$ | 15.87 | | 16.7 | 0.000 |

[a] Reference 3.
[b] Reference 4.

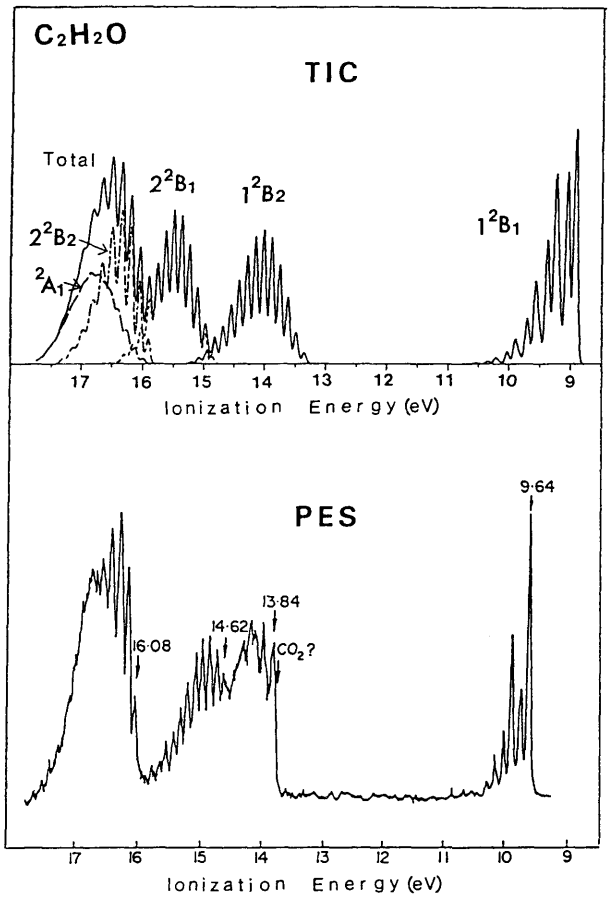


FIG. 1. The theoretical intensity curves of ionization of $C_2H_2O$ assuming a half width of 0.08 eV, which is compared with the observed PES by Turner *et al.* (Ref. 3). TIC: Theoretical intensity curve. PES: PE spectrum.

PES ranging from 14.6 eV to 16 eV. The 16–18 eV region of the TIC consists of two overlapping bands of the the $2\,^2B_2$ and $^2A_1$ states. The fine structure of this region is due to the vibrational progression of $2\,^2B_2$ whose vibrational structure is very similar to the observed PES.

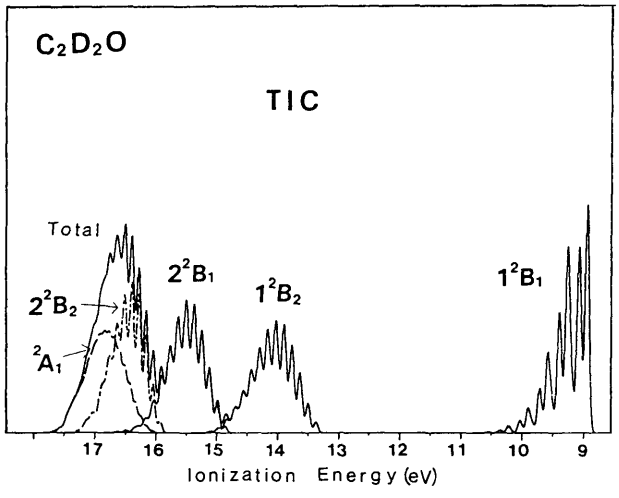


FIG. 2. The theoretical intensity curves of ionization of $C_2D_2O$ assuming a half width of 0.08 eV.

Figure 2 shows the overall feature of the TIC of $C_2D_2O$, which feature is very similar to the Fig. 1 of $C_2H_2O$. The observed PE spectrum of $C_2D_2O$ from Hall *et al.*[4] is also similar to that of $C_2H_2O$.

Turner *et al.* and Hall *et al.*[4] have reported the high-resolution PE spectrum for each state and assigned the vibrational frequencies. In order to discuss the assignment of vibrational structure, we calculated the theoretical intensity curve for each state with a half width of 0.04 eV. The results are shown in Figs. 3–10.

### A. 1 $^2B_1$ state

The theoretical intensity curve of ionization to the $1\,^2B_1$ state is shown in Fig. 3. The vibrational structure of the theoretical intensity curve is in good agreement with the PE spectrum.[3] The intensity of the O–O transition of TIC is weaker than that of PES. This situation should be connected that the calculated geometrical change by ionization may be overestimated. The vibrational levels are assigned in Fig. 3 where

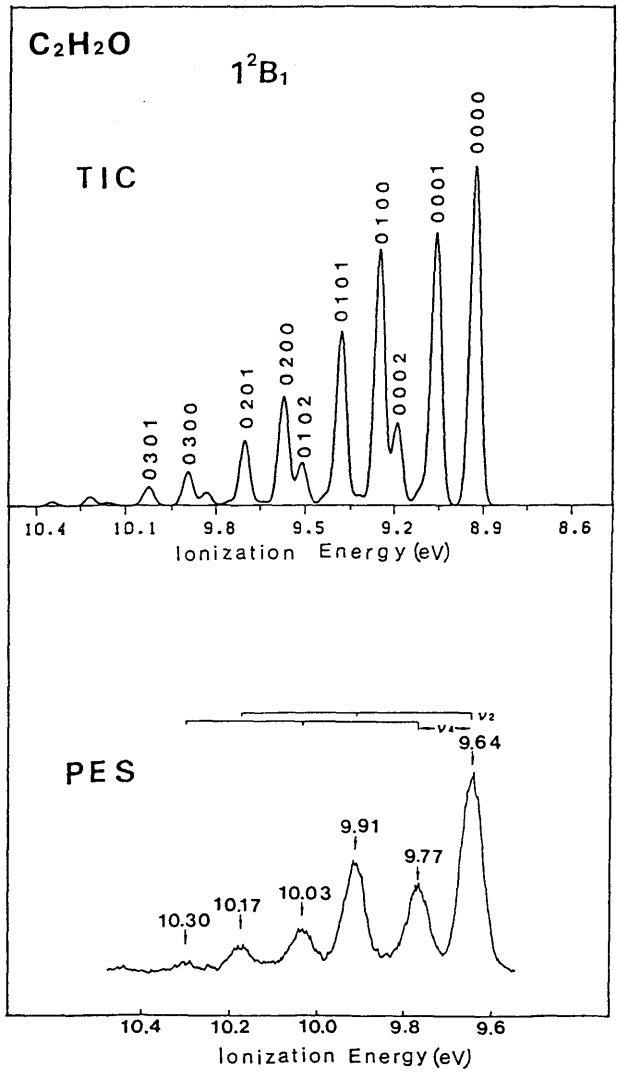


FIG. 3. The theoretical intensity curve of ionization to $1\,^2B_1$ of $C_2H_2O$ with a half width of 0.04 eV, which is compared with the observed PES by Turner *et al.* (Ref. 3).

TABLE X. Observed vibrational frequencies ($cm^{-1}$) and its assignment.

| | State | Observed frequency | | Assignment | | |
|---|---|---|---|---|---|---|
| | | Baker[a] | Hall[b] | Baker[a] | Hall[b] | This work |
| $CH_2O_2$ | $1\,^2B_1$ | 2140 | 2220 | $\nu_2$ | $\nu_2$ | $\nu_2$ |
| | | 1020 | 1080 | $\nu_4$ | $\nu_4$ | $\nu_4$ |
| | $1\,^2B_2$ | 1130 | | ? | | $\nu_4$ |
| | $2\,^2B_1$ | 940 | 950 | $\nu_3$ | $\nu_4$ | $\nu_4, \nu_2/2$ |
| | $2\,^2B_2$ | 1020 | 1020 | $\nu_3$ | $\nu_3$ | $\nu_4$ |
| $CD_2O_2$ | $1\,^2B_1$ | | 2220 | | $\nu_2$ | $\nu_1$ |
| | | | 1080 | | $\nu_4$ | $(\nu_3+\nu_4)/2$ |
| | $2\,^2B_1$ | | 950 | | $\nu_4$ | $(\nu_3+\nu_4)/2, \nu_2/2$ |
| | $2\,^2B_2$ | | 860 | | $\nu_3$ | $\nu_4$ |

[a] Reference 1.
[b] Reference 4.

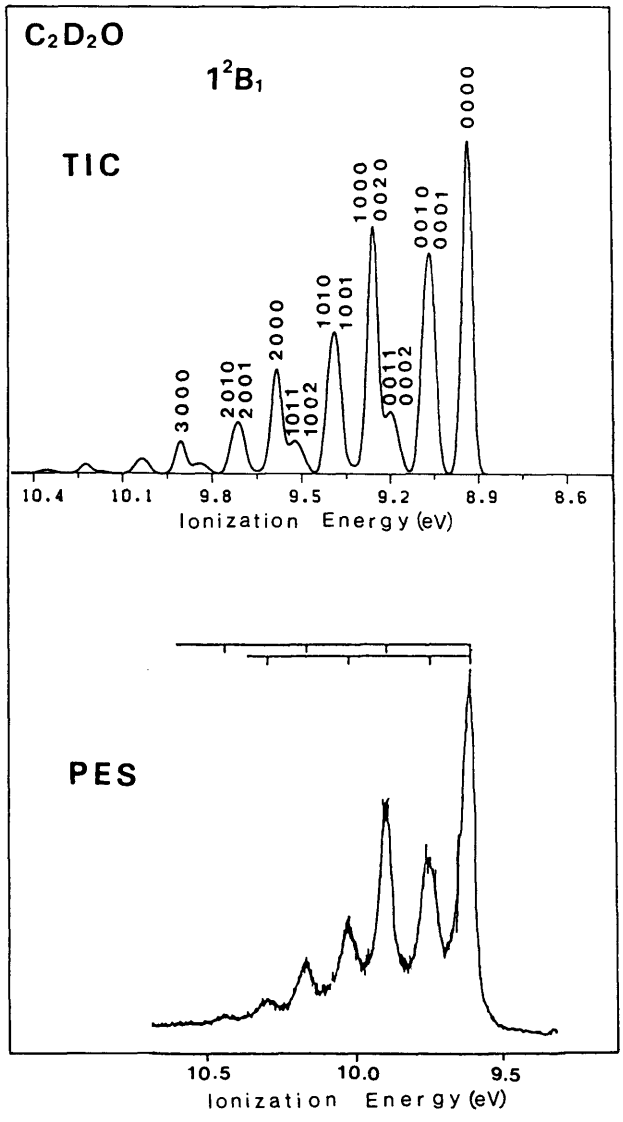


FIG. 4. The theoretical intensity curve of ionization to $1\,^2B_1$ of $C_2D_2O$ with a half width of 0.04 eV, which is compared with the observed PES by Hall *et al.* (Ref. 4).

the vibrational quantum numbers of the $\nu_1$, $\nu_2$, $\nu_3$, and $\nu_4$ modes are illustrated. The figure shows that the higher vibrational excitation of the $\nu_2$ (C = O stretching) and $\nu_4$ (C = C stretching) modes contribute to the intensity. The three vibrational progressions of ($v_2 = 0 \sim 3$), ($v_2 = 0 \sim 3$ and $v_4 = 1$), and ($v_2 = 0 \sim 1$ and $v_4 = 2$) are found. Turner *et al.* assigned the vibrational fine structure to a series of ($v_2 = 0 \sim 2$) and ($v_2 = 0 \sim 2$ and $v_4 = 1$). They neglected a series of ($v_2 = 0 \sim 1$ and $v_4 = 2$). From the analysis of PES, Baker *et al.*[1] have obtained the frequencies of $\nu_2$ and $\nu_4$ as 2140 and 1020 $cm^{-1}$, respectively (see Table X). Hall *et al.* assigned the frequencies of 2220 and 1080 $cm^{-1}$ to $\nu_2$ and $\nu_4$, respectively. The present calculated frequencies of $\nu_2$ and $\nu_4$ are 2596 and 1024 $cm^{-1}$, respectively. The calculated frequency of $\nu_2$ is overestimated by 17 or 20% and that of $\nu_4$ is almost the same value as the observed one. The third peak of PES was assigned to the transition to the vibrational level of (0 1 0 0) by Turner *et al.* The theoretical intensity curve shows that the third peak of PES corresponds to the vibrational levels of (0 1 0 0) and (0 0 0 2). The energy splitting between the two levels is estimated as 0.06 eV by the use of the calculated frequency. While using the observed frequency, the energy splitting is estimated as 0.01 eV which is smaller than resolvability of spectrum. Therefore, the third peak of PES should be superimposed by the two vibrational levels. This situation may be connected that the intensity of the third peak of PES is larger than that of the second peak.

Figure 4 shows the TIC of $C_2D_2O$ and the assignment of the vibrational levels. A weight of the intensity of the (0 0 1 0) and (0 0 0 1) levels is fifty–fifty from the FCF. The figure is very similar to the TIC of $C_2H_2O$. The figure shows that the higher vibrational excitation of the $\nu_1$, $\nu_3$, and $\nu_4$ modes contribute to the intensity. However, the character of the vibrational modes is not the same as that of $C_2H_2O$. The character of the $\nu_1$ is assigned to the C = O stretching mode of which calculated frequency is the same as that of the $\nu_2$ (C = O stretching) mode of $C_2H_2O$. For the $\nu_3$ and $\nu_4$ modes, we find a large coupling between the C = C stretching motion and the H–C = C bending motion. Table VI

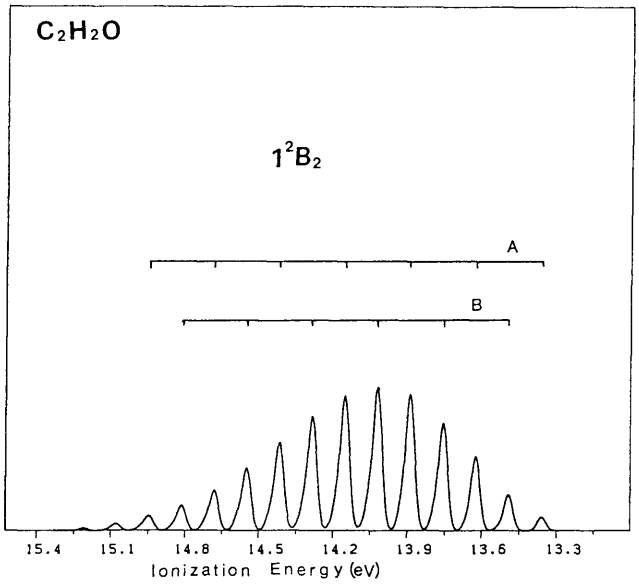


FIG. 5. The theoretical intensity curve of ionization to $1\ ^2B_2$ of $C_2H_2O$ with a half width of 0.04 eV.

shows that the phase of the linear combination of the C = C stretching and the H–C = C bending is out of phase for the $\nu_3$ mode and in phase for the $\nu_4$ mode. Hall *et al.* assigned the next frequencies of 2220 and 1080 $cm^{-1}$ to $\nu_2$ (C = O stretching) and $\nu_4$ (C = C stretching), respectively. Figure 4 shows that the frequency of 2220 $cm^{-1}$ corresponds to the (1 0 0 0) and (0 0 2 0) levels, and that the frequency 1080 $cm^{-1}$ corresponds to the (0 0 1 0) and (0 0 0 1) levels. Therefore, we should assign the frequency of 2220 $cm^{-1}$ to the $\nu_1$ mode (C = O stretching) of which calculated frequency is 2596 $cm^{-1}$. It should be also assigned to $2*\nu_3$. The observed frequency of 1080 $cm^{-1}$ should correspond to the average frequency of the $\nu_3$ and $\nu_4$ modes. The calculated frequencies of $\nu_3$ and $\nu_4$ are 1153 and 950 $cm^{-1}$, respectively.

TABLE XI. Vibrational levels of the $1\ ^2B_2$ state of $CH_2O_2$.

| IE | Vibrational level |
|---|---|
| Progression A | |
| 13.36 | (0 0 0 0) |
| 13.62-13.66 | (0 1 0 0),(0 0 0 2), (0 0 1 1) |
| 13.88-13.92 | (0 2 0 0),(0 1 0 2),(0 0 0 4),(0 1 1 1),(0 0 1 3) |
| 14.15-14.19 | (0 3 0 0),(0 2 0 2),(0 1 0 4),(0 2 1 1),(0 1 1 3) |
| 14.41-14.45 | (0 4 0 0),(0 3 0 2),(0 2 0 4),(0 3 1 1),(0 2 1 3) |
| 14.68-14.72 | (0 5 0 0),(0 4 0 2),(0 3 0 4),(0 4 1 1) |
| 14.95 | (0 5 0 2) |
| Progression B | |
| 13.49 | (0 0 0 1) |
| 13.76-13.79 | (0 1 0 1),(0 0 0 3),(0 1 1 0),(0 0 1 2) |
| 14.02-14.05 | (0 2 0 1),(0 1 0 3),(0 2 1 0),(0 1 1 2) |
| 14.28-14.32 | (0 3 0 1),(0 2 0 3),(0 3 1 0),(0 2 1 2) |
| 14.55-14.58 | (0 4 0 1),(0 3 0 3), (0 3 1 2) |
| 14.81 | (0 5 0 1),(0 4 0 3) |

### B. $1\ ^2B_2$ state

The theoretical intensity curve of ionization to the $1\ ^2B_2$ state in Fig. 5 shows well resolved vibrational structure. In the figure, we find the two vibrational progressions (A and B). The assignment of the vibrational levels of these progressions is presented in Table XI. The progression A consists of the vibrational excitations of the five series: ($v_2 = 0 \sim 5$), ($v_2 = 0 \sim 5$ and $v_4 = 2$), ($v_2 = 0 \sim 3$ and $v_4 = 4$), ($v_2 = 0 \sim 4$, $v_3 = 1$ and $v_4 = 1$), and ($v_2 = 0 \sim 2$, $v_3 = 1$, and $v_4 = 3$). The progression B consists of the vibrational excitations of the four series: ($v_2 = 0 \sim 5$ and $v_4 = 1$), ($v_2 = 0 \sim 4$ and $v_4 = 3$), ($v_2 = 1 \sim 3$ and $v_3 = 1$), and ($v_2 = 0 \sim 3$, $v_3 = 1$, and $v_4 = 2$). Although many series are concerned with the vibrational excitations, the theoretical intensity curve shows well resolved vibrational structure. This situation is connected to the following relation of the calculated vibrational frequencies: $\nu_2 \simeq 2\nu_4$ and $\nu_2 \simeq \nu_3 + \nu_4$. The peak separation of each vibrational progression is connected to the $\nu_2$ mode and that between two progressions is attributed to the $\nu_4$ mode. The present calculation reveals that the higher vibrational excitation of the $\nu_2$ mode contributes to the intensity. This feature is associated with the change in the equilibrium molecular structure by ionization and vibrational mode. The change in the C = O bond distance ( + 0.155 Å) and C = C bond distance ( − 0.050 Å) is large by comparison with the classical half amplitude. Therefore, the vibrational excitation of such a mode as lengthening the C = O bond distance and shortening the C = C bond distance contributes to the intensity. Table VI indicates that the $\nu_2$ mode (C = C = O out-of-phase stretching) is suitable for such a condition.

The observed PES shows more complicated vibrational structure compared with the present TIC. Hall *et al.* expected that the complexity of the band may be a result of predissociation of ketene. However, the present study shows that the $1\ ^2B_2$ state is stable. The complexity may be attributed to the disappearance of the fine structure of PES because of the superimposition of peaks associated with $CO_2$ band near 13.8 eV and with the third band of $C_2H_2O$ above 14.6 eV. The complexity may be attributed to inadequacy of the theoretical approximation method. In order to check the stability of the molecular structure of $C_{2v}$ symmetry, we optimized it with $C_s$ symmetry. The result shows that the structure of $C_{2v}$ symmetry is a true equilibrium. The well resolve fine structure of TIC is ascribed to the relation of the calculated vibrational frequencies ($\nu_2 \simeq 2\nu_4$ and $\nu_2 \simeq \nu_3 + \nu_4$). If the above condition does not exist due to the anharmonic effect, the theoretical intensity curve should be more complicated.

Turner *et al.* obtained the vibrational frequency of 1130 $cm^{-1}$ from the vibrational spacing of the second band of PES. However, they did not assign the vibrational mode. The theoretical intensity curve shows that the peak separation of the vibrational progressions is ascribed to the $\nu_4$ mode (1057 $cm^{-1}$, C = C = O in-phase stretching). Therefore, we should assign the frequency of 1130 $cm^{-1}$ to the $\nu_4$ mode.

Figure 6 shows the TIC of $C_2D_2O$. Table XII shows the vibrational levels for each peak. Comparing with $C_2D_2O$ and $C_2H_2O$, we notice that higher vibrational excitation of

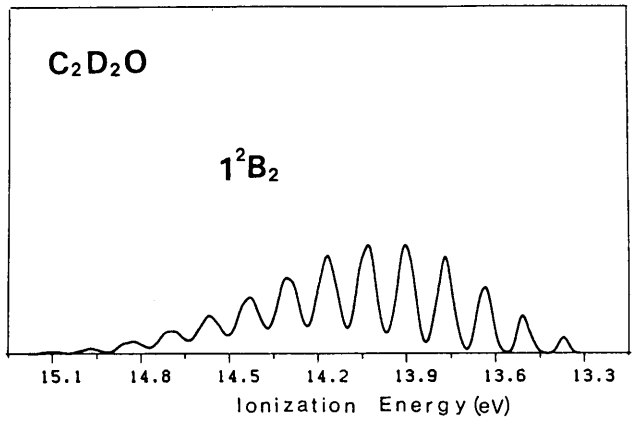


FIG. 6. The theoretical intensity curve of ionization to $1\,^2B_2$ of $C_2D_2O$ with a half width of 0.04 eV.

the $\nu_1$ mode contribute to intensity in addition to the $\nu_2$, $\nu_3$, and $\nu_4$ modes. This situation is ascribed to a change of the character of the $\nu_1$ mode where a component of the C = C stretching motion appears. Although all vibrational modes contribute to the intensity, the TIC shows well resolved vibrational structure. This ascribes to the following relation of the calculated vibrational frequencies: $\nu_1 \simeq \nu_2$, $\nu_3 \simeq \nu_4$ and, $\nu_1 \simeq 2\nu_3$.

### C. $2\,^2B_1$ state

The theoretical intensity curve of ionization to the $2\,^2B_1$ state is illustrated in Fig. 7 and compared with the observed PES.[3] The third peak of TIC may correspond with the observed peak at 14.62 eV which have been assigned to the O–O IE. Therefore, the O–O IE of $2\,^2B_1$ should be lower than the observed value of 14.62 eV. It may be 14.38 eV.

The theoretical intensity curve shows the two vibrational progressions of A and B of which vibrational levels are assigned in Table XIII. The vibrational progressions A which has strong intensity consists of the vibrational excitations of the four series: ($v_4 = 0 \sim 7$), ($v_2 = 1$ and $v_4 = 0 \sim 7$), ($v_2 = 2$ and $v_4 = 1 \sim 6$), and ($v_2 = 3$ and $v_4 = 1 \sim 4$). The vibrational progressions B of weak intensity is connected to the vibrational excitations of the three series: ($v_3 = 1$ and $v_4 = 1 \sim 6$), ($v_2 = 1$, $v_3 = 1$, and $v_4 = 1 \sim 5$), and ($v_2 = 2$, $v_3 = 1$, and $v_4 = 2 \sim 4$). The contribution of the higher vibrational excitations of the $\nu_4$ (C = C = O in-

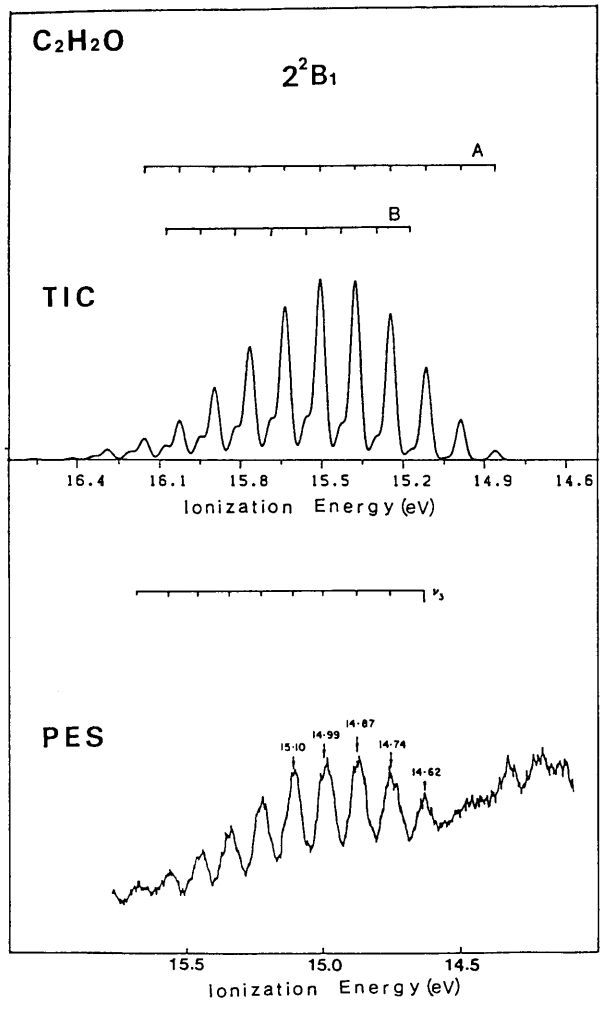


FIG. 7. The theoretical intensity curve of ionization to $2\,^2B_1$ of $C_2H_2O$ with a half width of 0.04 eV, which is compared with the observed PES by Turner *et al.* (Ref. 3).

TABLE XII. Vibrational levels of the $1\,^2B_2$ state of $CD_2O_2$.

| IE | Vibrational level |
|---|---|
| 13.37 | (0 0 0 0) |
| 13.51 | (0 0 1 0) |
| 13.62-13.65 | (0 0 1 1),(0 1 0 0),(0 0 2 0) |
| 13.74-13.80 | (0 1 0 1),(0 0 2 1),(0 1 1 0),(0 0 3 0),(1 0 1 0) |
| 13.88-13.94 | (0 1 1 1),(0 2 0 0),(0 1 2 0),(1 1 0 0),(1 0 2 0) |
| 14.02-14.06 | (0 1 2 1),(0 2 1 0),(0 1 3 0),(1 1 1 0) |
| 14.13-14.20 | (0 2 1 1),(0 2 2 0),(1 1 1 1),(1 2 0 0),(1 1 2 0) |
| 14.27-14.32 | (0 2 2 1),(0 3 1 0),(0 2 3 0),(1 1 2 1),(1 2 1 0) |
| 14.42-14.46 | (0 3 2 0),(1 2 2 0) |

TABLE XIII. Vibrational levels of the $2\,^2B_1$ state of $CH_2O_2$.

| IE | Vibrational level |
|---|---|
| Progression A | |
| 14.86 | (0 0 0 0) |
| 14.99 | (0 0 0 1) |
| 15.12-15.12 | (0 0 0 2), (0 1 0 0) |
| 15.24-15.25 | (0 0 0 3), (0 1 0 1) |
| 15.37-15.38 | (0 0 0 4), (0 1 0 2) |
| 15.50-15.51 | (0 0 0 5), (0 1 0 3), (0 2 0 1) |
| 15.63-15.64 | (0 0 0 6), (0 1 0 4), (0 2 0 2) |
| 15.76-15.78 | (0 0 0 7), (0 1 0 5), (0 2 0 3), (0 3 0 1) |
| 15.91 | (0 1 0 6), (0 2 0 4), (0 3 0 2) |
| 16.03 | (0 1 0 7), (0 2 0 5), (0 3 0 3) |
| 16.16 | (0 2 0 6), (0 3 0 4) |
| Progression B | |
| 15.17 | (0 0 1 1) |
| 15.30 | (0 0 1 2) |
| 15.43 | (0 0 1 3), (0 1 1 1) |
| 15.55-15.56 | (0 0 1 4), (0 1 1 2) |
| 15.68-15.69 | (0 0 1 5), (0 1 1 3) |
| 15.81-15.83 | (0 0 1 6), (0 1 1 4), (0 2 1 2) |
| 15.95 | (0 1 1 5), (0 2 1 3) |
| 16.08 | (0 2 1 4) |

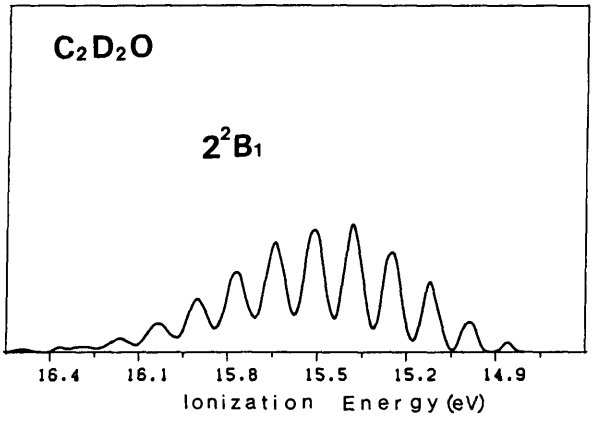


FIG. 8. The theoretical intensity curve of ionization to $2\,^2B_1$ of $C_2D_2O$ with a half width of 0.04 eV.

phase stretching) mode is associated with lengthening of the C = C bond distance ( + 0.041 Å) and the C = O bond distance ( + 0.135 Å) by ionization.

Turner *et al.* reported that the peak separations of the third band corresponded to a vibrational frequency of 940 $cm^{-1}$. They assigned it to the $\nu_3$ mode. Hall *et al.* suggested that the excitation was the $\nu_4$ mode from the equivalence of band in ketene-$d_2$. Table XIII shows that the vibrational spacing of the progression A with strong intensity is due to the $\nu_4$ mode of which vibrational frequency is 1033 $cm^{-1}$. Thus, present calculation supports the assignment by Hall *et al.* Table XIII also indicates that the vibrational progression by the excitation of the $\nu_2$ mode superimposes on that by the $\nu_4$ mode, because the calculated vibrational frequency of the $\nu_2$ mode (2125 $cm^{-1}$) is almost twice that of the $\nu_4$ mode (1033 $cm^{-1}$). Therefore, we expect that the vibrational frequency of the $\nu_2$ mode should be about 1880 $cm^{-1}$ by the use of the observed frequency of the $\nu_4$ mode (940 $cm^{-1}$).

Figure 8 shows the TIC of $C_2D_2O$. Table XIV shows the vibrational levels for each peak. A weight of the intensity of the (0 0 0 1) and (0 0 1 0) levels is fifty–fifty from the FCF. Higher vibrational excitations of the $\nu_2$, $\nu_3$, and $\nu_4$ modes contribute to intensity. The character of the $\nu_2$ mode is assigned to the C = C = O out-of-phase stretching mode from Table VIII. The $\nu_3$ and $\nu_4$ modes are found coupling between the C = C = O in-phase stretching motion and the H–C = C bending motion. Hall *et al.* assigned the peak separations of 950 $cm^{-1}$ to the $\nu_4$ mode. The peak separations of the TIC is about 1000 $cm^{-1}$. This separation corresponds to the frequency of the average value between the $\nu_3$ and $\nu_4$ modes. Table XIV indicates that the $\nu_2$ mode also contributes to the intensity. The calculated frequency of $\nu_2$ is 2111 $cm^{-1}$, which is twice of the average value between the $\nu_3$ and $\nu_4$ modes. Therefore, we expect that the observed frequency of 950 $cm^{-1}$ should be the average value between the $\nu_3$ and $\nu_4$ modes and half value of the $\nu_2$ mode.

TABLE XIV. Vibrational levels of the $2\,^2B_1$ state of $CD_2O_2$.

| IE | Vibrational level |
|---|---|
| 14.86 | (0 0 0 0) |
| 14.97-15.00 | (0 0 0 1),(0 0 1 0) |
| 15.09-15.15 | (0 0 0 2),(0 0 1 1),(0 0 2 0),(0 1 0 0) |
| 15.20-15.29 | (0 0 0 3),(0 0 1 2),(0 1 0 1),(0 0 2 1),(0 1 1 0), (0 0 3 0) |
| 15.35-15.41 | (0 0 1 3),(0 1 0 2),(0 0 2 2),(0 1 1 1),(0 0 3 1), (0 1 2 0) |
| 15.46-15.56 | (0 0 1 4),(0 1 0 3),(0 0 2 3),(0 1 1 2),(0 0 3 2), (0 1 2 1),(0 1 3 0) |
| 15.61-15.67 | (0 1 1 3),(0 0 3 3),(0 1 2 2),(0 2 1 1),(0 1 3 1) |
| 15.76-15.79 | (0 1 2 3),(0 2 1 2),(0 1 3 2),(0 2 2 1) |
| 15.90 | (0 2 2 2), |

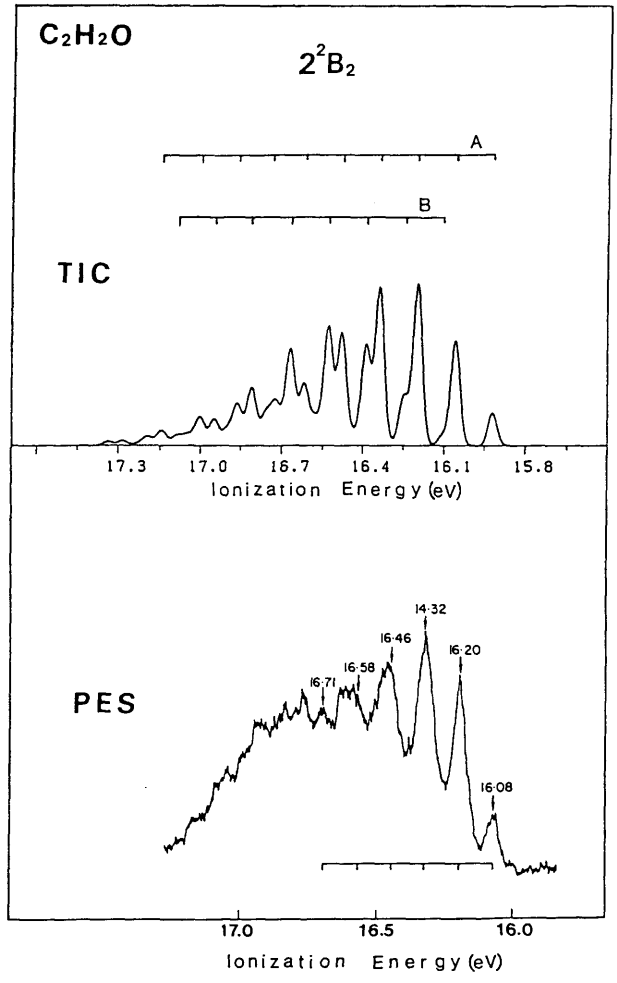


FIG. 9. The theoretical intensity curve of ionization to $2\,^2B_2$ of $C_2H_2O$ with a half width of 0.04 eV, which is compared with the fourth band of the observed PES by Turner *et al.* (Ref. 3).

### D. $2\,^2B_2$ state

The 16–18 eV region of the PES consists of the two overlapping bands of the ionization to the $2\,^2B_2$ and $^2A_1$ states. The present calculation reveals that the TIC of $2\,^2B_2$ shows a resolved vibrational structure and that of $^2A_1$ shows continuous feature. Therefore, the fine structure of this region is due to the vibrational progression from the ionization to $2\,^2B_2$.

The theoretical intensity curve of ionization to the $2\,^2B_2$ state is illustrated in Fig. 9 and compared with the observed

TABLE XV. Vibrational levels of the $2\,^2B_2$ state of $CH_2O_2$.

| IE | Vibrational level |
|---|---|
| Progression A | |
| 15.92 | (0 0 0 0) |
| 16.06 | (0 0 0 1) |
| 16.20 | (0 0 0 2) |
| 16.34 | (0 0 0 3) |
| 16.43-16.48 | (0 0 0 4), (0 1 1 0) (0 0 2 1) |
| 16.57-16.62 | (0 0 0 5), (0 1 1 1), (0 2 0 0), (0 0 2 2) |
| 16.71-16.76 | (0 0 0 6), (0 1 1 2), (0 2 0 1), (0 0 2 3) |
| 16.85-16.90 | (0 0 0 7), (0 1 1 3), (0 2 0 2), (0 0 2 4) |
| 17.00-17.01 | (0 1 1 4), (0 2 0 3) |
| 17.14-17.15 | (0 1 1 5), (0 2 0 4) |
| Progression B | |
| 16.11 | (0 0 1 0) |
| 16.25-16.25 | (0 0 1 1), (0 1 0 0) |
| 16.39-16.39 | (0 0 1 2), (0 1 0 1) |
| 16.53-16.53 | (0 0 1 3), (0 1 0 2) |
| 16.66-16.67 | (0 0 1 4), (0 1 0 3) |
| 16.80-16.81 | (0 0 1 5), (0 1 0 4) |
| 16.94-16.95 | (0 0 1 6), (0 1 0 5) |
| 17.09 | (0 1 0 6) |

TABLE XVI. Vibrational levels of the $2\,^2B_2$ state of $CD_2O_2$.

| IE | Vibrational level |
|---|---|
| Progression A | |
| 15.93 | (0 0 0 0) |
| 16.05 | (0 0 0 1) |
| 16.16 | (0 0 0 2) |
| 16.28 | (0 0 0 3) |
| 16.39-16.40 | (0 0 0 4), (1 0 0 1) |
| 16.51 | (0 0 0 5), (1 0 0 2) |
| 16.62-16.63 | (0 0 0 6), (1 0 0 3) |
| 16.74-16.75 | (0 0 0 7), (1 0 0 4) |
| 16.86 | (0 0 0 8) |
| Progression B | |
| 16.32-16.33 | (0 0 1 2), (0 1 0 1) |
| 16.44 | (0 0 1 3), (0 1 0 2) |
| 16.55-16.56 | (0 0 1 4), (0 1 0 3) |
| 16.68 | (0 1 0 4) |
| 16.79 | (0 1 0 5) |
| 16.91 | (0 1 0 6) |
| 17.03 | (0 1 0 7) |

PES.[3] The first peak of TIC should correspond with the observed peak at 16.08 eV which have been assigned to the O–O IE of the fourth band. The two vibrational progressions (A and B) are found. Table XV shows the assignment of the vibrational levels of these progressions. The vibrational progressions of A, which has strong intensity in the lower energy region, consists of the vibrational excitations of the four series: ($v_4 = 0 \sim 7$), ($v_2 = 1$, $v_3 = 1$, and $v_4 = 0 \sim 5$), ($v_2 = 2$ and $v_4 = 0 \sim 4$), and ($v_2 = 2$ and $v_4 = 1 \sim 4$). The vibrational progressions B which has large intensity in the higher energy side consists of the vibrational excitations of the two series: ($v_3 = 1$ and $v_4 = 0 \sim 6$) and ($v_2 = 1$ and $v_4 = 0 \sim 6$). The present calculation reveals that the higher vibrational excitation of the $\nu_4$ mode contributes to the intensity. The contribution of the higher vibrational excitations of $\nu_4$ (mixture of the C = C = O in-phase stretching and H–C = C bending motions with in-phase mode) is ascribed to the large geometrical change in the C = O bond distance ( + 0.094 Å) and H–C = C angle ( + 8.92°).

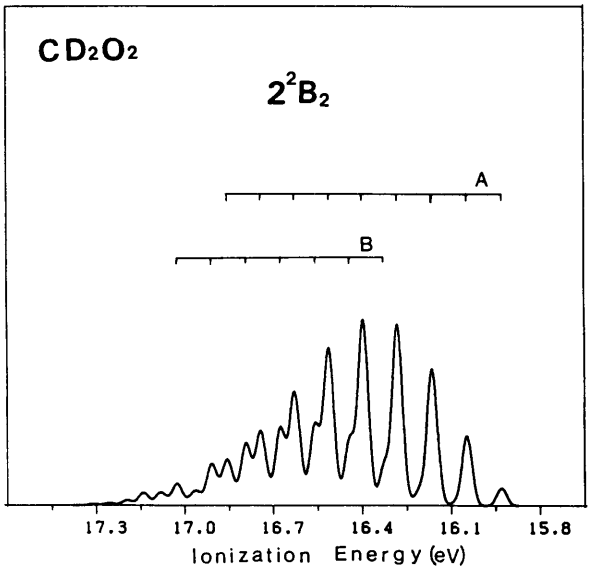


FIG. 10. The theoretical intensity curve of ionization to $2\,^2B_2$ of $C_2D_2O$ with a half width of 0.04 eV.

From the analysis of the vibrational structure in the lower energy side of the fourth band, Turner *et al.* found that the vibrational spacing corresponded to a frequency of 1020 $cm^{-1}$ and assigned it to the $\nu_3$ mode ($CH_2$ deformation). Hall *et al.* supported this assignment from the analysis of spectrum of ketene-$d_2$. However, the present calculation reveals that vibrational spacing of the progression A is ascribed to the $\nu_4$ mode in the lower energy side (see Table XV). Therefore, we assigned the observed frequency to the $\nu_4$ mode. The calculated frequency of the $\nu_4$ mode is 1127 $cm^{-1}$, whereas that of the $\nu_3$ mode (mixture of C = C stretching and H–C = C bending with out-of-phase mode) is 1503 $cm^{-1}$.

Figure 10 shows the TIC of $C_2D_2O$. The two vibrational progressions (A and B) are found. Table XVI shows the assignment of the vibrational levels of these progressions. The vibrational progressions of A, which has strong intensity in the lower energy region, consists of the vibrational excitations of the $\nu_4$ mode. The character of the $\nu_4$ mode is a mixture of the in-phase motions of the C = O stretching and H–C = C bending. The observed PES shows well resolved vibrational structure in the lower energy side. Hall *et al.* assigned the observed frequency of 860 $cm^{-1}$ to the $\nu_3$ ($CH_2$ deformation) mode. The calculated frequencies of the $\nu_3$ and $\nu_4$ modes are 1263 and 940 $cm^{-1}$, respectively. We should assign the observed frequency to the $\nu_4$ mode.

### E. $^2A_1$ state

The theoretical intensity curve of the $^2A_1$ state shows continuous spectrum. This feature is connected to the nature

of the vibrational excited levels. The present calculation reveals that the vibrational levels consist of such series as ($v_4 = 2 \sim 8$), ($v_3 = 1$ and $v_4 = 1 \sim 8$), ($v_3 = 2$ and $v_4 = 1 \sim 7$), ($v_3 = 3$ and $v_4 = 2 \sim 6$), ($v_1 = 1$ and $v_4 = 2 \sim 7$), ($v_1 = 1$, $v_3 = 1$, and $v_4 = 2 \sim 7$), ($v_1 = 1$, $v_3 = 2$, and $v_4 = 2 \sim 7$), ($v_1 = 1$, $v_3 = 3$, and $v_4 = 3 \sim 5$), and ($v_1 = 2$, $v_3 = 1$, and $v_4 = 3 \sim 5$). The calculated spacing of those vibrational progression is estimated about 0.04 eV which corresponds to the difference of frequency between $\nu_3$ and $\nu_4$. Therefore, the TIC with a half width of 0.08 eV shows continuous spectrum.

The present calculation shows that the VIE and O–O IE are 16.98 and 15.87 eV, respectively. Hall *et al.* reported that the VIE and O–O IE were 16.8 and 16.7 eV, respectively. The deviation between the calculated and the observed O–O IEs is large comparing with other states. The energy lowering of the O–O IE from the VIE is 0.1 eV of which value is very small comparing with the calculated one (1.11 eV). A large geometric change in the H–C = C bond angle of the $^2A_1$ state causes a large energy lowering of the O–O IE from the VIE and a broad band shape of PES. The calculated FCF of the O–O transition is very small and the PES of $^2A_1$ overlaps that of $2\,^2B_2$. It should be impossible to determine clearly the O–O IE of $^2A_1$ from PES. Therefore, Hall *et al.* should miss the assignment of the O–O IE.

## IV. CONCLUSION

The molecular equilibrium structure and the vibrational frequency are calculated for the ground and lower five ionic states. By the use of the FCFs, we obtain transition intensity curve. The vibrational structure of the theoretical intensity curve is in good agreement with that of the observed PE spectrum except for the $1\,^2B_2$ state. The assignment of the observed vibrational frequencies is summarized in Table X. A number of new results for the vibrational levels are as follows.

For the $1\,^2B_1$ state, the third peak of the PES of $C_2H_2O$ should be superimposed by the vibrational levels of (0 1 0 0) and (0 0 0 2). The observed frequency of 2220 $cm^{-1}$ of $C_2D_2O$ should be also assigned to the $\nu_1$ mode of which character is the C = O stretching mode. The observed frequency of 1080 $cm^{-1}$ of $C_2D_2O$ should correspond to the average frequency of the $\nu_3$ and $\nu_4$ modes. The character of the $\nu_3$ and $\nu_4$ modes are a mixture of the C = C stretching and the H–C = C bending with out-of-phase mode and with in-phase mode, respectively.

For the $1\,^2B_2$ state, the observed vibrational spacing (1130 $cm^{-1}$) of $C_2H_2O$ is due to the $\nu_4$ mode (C = C = O in-phase stretching).

The O–O IE of $2\,^2B_1$ of $C_2H_2O$ should be lower than the observed value of 14.62 eV. It may be 14.38 eV. The well resolved vibrational progression of the $2\,^2B_1$ state of $C_2H_2O$ is ascribed to the vibrational excitations of the four series: ($v_4 = 0 \sim 7$), ($v_2 = 1$ and $v_4 = 0 \sim 7$), ($v_2 = 2$ and $v_4 = 1 \sim 6$), and ($v_2 = 3$ and $v_4 = 1 \sim 4$). The present study supports the assignment by Hall *et al.* who assigned the observed peak separations (940 $cm^{-1}$) to the $\nu_4$ mode. We also expect that the vibrational frequency of the $\nu_2$ mode should be about 1880 $cm^{-1}$ of which the value is twice of $\nu_4$, because the vibrational progression due to the excitation of the $\nu_2$ mode superimposes on that of the $\nu_4$ mode. The observed frequency of 950 $cm^{-1}$ of $C_2D_2O$ should be the average value between the $\nu_3$ and $\nu_4$ modes and half value of the $\nu_2$ mode. The character of the $\nu_2$ mode is the C = C = O out-of-phase stretching mode. The $\nu_3$ and $\nu_4$ modes are found coupling between the C = C = O in-phase stretching motion and the H–C = C bending motion.

The 16–18 eV region of the PES consists of the two overlapping bands of the ionization to the $2\,^2B_2$ and $^2A_1$ states. The resolved vibrational structure of PES is attributed to the $2\,^2B_2$ state. The TIC of $^2A_1$ shows continuous feature. The observed vibrational spacing (1020 $cm^{-1}$) of $C_2H_2O$ is assigned to the $\nu_4$ mode (mixture of the C = C = O in-phase stretching and H–C = C bending motions with in-phase mode). The observed frequency of 860 $cm^{-1}$ of $C_2D_2O$ should be assigned to the $\nu_4$ mode (mixture of the in-phase motions of the C = O stretching and H–C = C bending).

## ACKNOWLEDGMENT

Computation was carried out on HITAC M-680H systems at the Center for Information Processing Education of Hokkaido University.

[1] A. D. Baker and D. W. Turner, Chem. Commun. 480 (1969).
[2] D. W. Turner, Philos. Trans. R. Soc. London Ser. A **7**, 268 (1970).
[3] D. W. Turner, A. D. Baker, C. Baker, and C. R. Brundle, *Molecular Photoelectron Spectroscopy* (Wiley, London, 1970).
[4] D. Hall, J. P. Maier, and P. Rosmus, Chem. Phys. **373**, 24 (1977).
[5] D. P. Chong, Theor. Chim. Acta **181**, 50 (1978).
[6] K. Kimura, S. Katsumata, Y. Achiba, T. Yamazaki, and S. Iwata, *Handbook of HeI Photoelectron Spectra of Fundamental Organic Molecules* (Halsted, New York, 1981).
[7] G. D. Alti, P. Decleva, and A. Lisini, Chem. Phys. **185**, 76 (1983).
[8] H. Huber and J. Vogt, Chem. Phys. **399**, 64 (1982).
[9] R. D. Brown, E. H. N. Rice, and M. Rodler, Chem. Phys. **347**, 99 (1985).
[10] J. L. Duncan, A. M. Ferguson, J. Haroer, and K. H. Tonge, J. Mol. Spectrosc. **196**, 125 (1987).
[11] W. D. Allen and H. F. Schaefer III, J. Chem. Phys. **87**, 7076 (1987).
[12] H. Tatewaki and S. Huzinaga, J. Comput. Chem. **1**, 205 (1980).
[13] A. D. Mclean and B. Liu, J. Chem. Phys. **58**, 1066 (1973).
[14] T. Shoda, T. Noro, T. Nomura, and K. Ohno, Int. J. Quantum Chem. **30**, 289 (1986).
[15] K. Takeshita., J. Chem. Phys. **86**, 329 (1987).
[16] K. Takeshita and F. Sasaki, 1981 Library program at the Hokkaido University Computing Center (in Japanese).
[17] H. Kashiwagi, T. Takada, E. Miyoshi, and S. Obara for the Library program at the Hokkaido University Computing Center, 1977 (in Japanese).
[18] K. Takeshita and F. Sasaki, 1990 Library program at the Hokkaido University Computing Center (in Japanese).
[19] A. Murakami, H. Iwaki, H. Terashima, T. Shoda, T. Kawaguchi, and T. Noro, Library program at the Hokkaido University Computing Center, 1986 (in Japanese).
[20] G. Herzberg, *Molecular Spectra and Molecular Structure, Part III*, (van Nostrand, New York, 1966).
[21] C. B. Moore and G. C. Pimental, J. Chem. Phys. **38**, 2816 (1963).